HIGH SPOTS FOR THE ICE-FISHING PROBLEM WITH SURFACE TENSION*

NATHAN WILLIS † , CHEE HAN TAN ‡ , CHRISTEL HOHENEGGER † , AND BRAXTON OSTING †

Abstract. In the ice-fishing problem, a half-space of fluid lies below an infinite rigid plate ("the ice") with a hole. We investigate the ice-fishing problem including the effects of surface tension on the free surface. The dimensionless number that describes the effect of surface tension is called the Bond number. For holes that are infinite parallel strips or circular holes, we transform the problem to an equivalent eigenvalue integro-differential equation on an interval and expand in the appropriate basis (Legendre and radial polynomials, respectively). We use computational methods to demonstrate that the high spot, i.e., the maximal elevation of the fundamental sloshing profile, for the ice-fishing problem is in the interior of the free surface for large Bond numbers, but for a sufficiently small Bond number the high spot is on the boundary of the free surface. While several papers have proven high spot results in the absence of surface tension as it depends on the shape of the container, to the best of our knowledge, this is the first study investigating the effects of surface tension on the location of the high spot.

Key words. fluid sloshing, surface tension, high spots conjecture, generalized eigenvalue problem, orthogonal polynomials

MSC codes. 76B10, 76B45, 65R15, 33C45, 45C05, 35P15, 47G20

DOI. 10.1137/21M1458879

1. Introduction. Sloshing refers to the motion of a liquid free surface, i.e., the interface between the liquid in the container and the air above, inside partially filled containers [13, 7]. Liquid sloshing is a ubiquitous phenomenon, ranging from the oscillation of fuel in road tank vehicles and liquid-propellant rockets to seiches in lakes and harbors induced by earthquakes to our everyday experience in carrying a cup of coffee. Liquid sloshing has detrimental impacts on the stability and structural safety of stationary or moving vessels. For example, violent fuel sloshing within spacecraft fuel tanks produces highly localized pressure on tank walls, leading to deviation from its planned flight path or compromising its structural integrity.

Surface tension, defined as a force per unit length, is the intermolecular force required to contract the liquid surface to its minimal surface area. Examples of surface tension effects include the nearly spherical shape of liquid droplets and the ability of small insects to walk on water. The dimensionless parameter measuring the relative magnitudes of gravitational and surface tension forces is referred to as the Bond number and given by Bo = $\rho g \ell_c^2/\sigma$, where $\rho > 0$ is the constant fluid density, ℓ_c is a characteristic length scale of the container, and $\sigma > 0$ is the surface tension coefficient. For example, in a microgravity environment, the magnitude of body forces is tiny, and surface tension forces predominate. Mathematically, surface tension is incorporated into the sloshing model via the Young-Laplace equation, $\Delta P = -2\sigma H$,

^{*}Received by the editors November 11, 2021; accepted for publication (in revised form) March 18, 2022; published electronically July 26, 2022.

 $[\]rm https://doi.org/10.1137/21M1458879$

Funding: The work of the second and fourth authors was partially supported by NSF DMS 17-52202.

[†]Department of Mathematics, University of Utah, Salt Lake City, UT 84112 USA (willis@math.utah.edu, choheneg@math.utah.edu, osting@math.utah.edu).

[‡]Department of Mathematics, Wake Forest University, Winston-Salem, NC 27109 USA (tanch@wfu.edu).

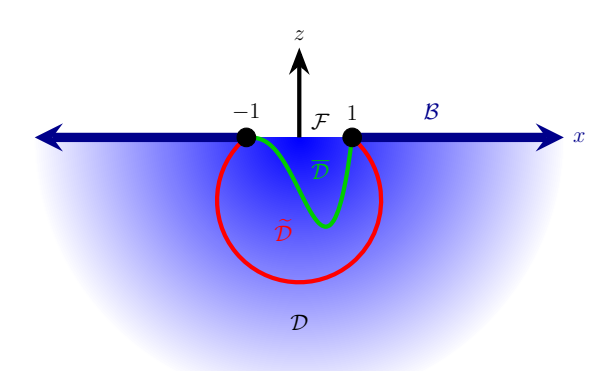


FIG. 1. An illustration of the fluid domain \mathcal{D} and boundary $\mathcal{B} \cup \mathcal{F} \cup \partial \mathcal{F}$ for a cross section of the infinite parallel strip IFP. Multiple bounded domains are shown to demonstrate the domain monotonicity property for the squared fundamental sloshing frequency, i.e., $\omega_1^2(\overline{\mathcal{D}}) \leq \omega_1^2(\widetilde{\mathcal{D}})$.

which asserts that the pressure difference ΔP between the inside and the outside of the fluid free surface is proportional to the mean surface curvature H. Recently a variational characterization of fluid sloshing with surface tension was derived in [26], and an isoperimetric problem was considered in [27].

In this paper, we investigate the ice-fishing problem (IFP), including the effects of surface tension on the free surface. The IFP studies the problem of free oscillations of an incompressible, inviscid fluid for an irrotational flow in a half-space bounded above by an infinite rigid plane, where the free surface is some aperture in the plane; see Figure 1. We consider the cases where the aperture is either a circular hole or an infinite parallel strip. We denote the equilibrium free surface by \mathcal{F} , the boundary of \mathcal{F} by $\partial \mathcal{F}$, the wetted boundary by \mathcal{B} , and the fluid domain by \mathcal{D} .

1.1. Previous results. In the absence of surface tension, Moiseev [21] established the property of domain monotonicity for the square of the fundamental (smallest) sloshing frequency ω_1^2 . Namely, for any two bounded containers $\overline{\mathcal{D}}, \widetilde{\mathcal{D}}$ with an identical \mathcal{F} and $\overline{\mathcal{D}} \subset \widetilde{\mathcal{D}}$, we have that $\omega_1^2(\overline{\mathcal{D}}) \leq \omega_1^2(\widetilde{\mathcal{D}})$; see Figure 1. This result is an immediate consequence of the variational characterization of ω_1^2 . It follows that the fundamental sloshing frequency for the IFP furnishes the universal upper bound for the fundamental sloshing frequency of arbitrary containers with coinciding \mathcal{F} . In the presence of surface tension, it was shown that this domain monotonicity result continues to hold for a free surface that is freely allowed to move at its boundary [26].

The IFP with zero surface tension has been well studied in the past few decades. Davis [5] reformulated the infinite parallel strip problem as an integral equation involving Green's function. He expressed the velocity potential as the infinite sum of Legendre polynomials and applied the principle of deformation of contours to give $\{\omega_j^2\}_{j=1}^{\infty}$ as the eigenvalues of an infinite symmetric matrix. Furthermore, he obtained approximations for ω_j^2 by computing the eigenvalues of the truncated matrix and derived a fourth-order asymptotic expansion for higher eigenvalues. Henrici, Troesch, and Wuytack [10] formulated the IFP with a circular or strip-like aperture including a decay condition at infinity for the fluid velocity field and derived an equivalent Fredholm integral equation for the velocity potential in the aperture using potential theory. Miles [20] recast the IFP as formulated by Henrici, Troesch, and Wuytack [10] to a homogeneous Fredholm integral equation for the velocity distribution in the

aperture. Troesch [28] transformed the IFP onto a bounded domain using the Kelvin inversion. Fox and Kuttler [8] transformed the infinite parallel strip problem into an equivalent weighted problem on a semi-infinite strip employing a conformal map. Most authors computed upper bounds for ω_j^2 on their equivalent problems using the Rayleigh–Ritz method. Kozlov and Kuznetsov [15] adopted the formulation from Henrici, Troesch, and Wuytack [10] and Miles [20] and studied the dependence of the fundamental sloshing frequency on the aperture's geometry, including a detailed investigation of the IFP with a circular hole.

Of particular interest is the problem of determining the location of high spots, i.e., the maximal elevation of the sloshing profile ξ . Unless otherwise noted, when discussing the high spots it is assumed that ξ is the fundamental sloshing profile. The study of these high spots is motivated as a fluid-analogue to the hot spots conjecture: "For any second eigenfunction of the Neumann Laplacian, the extremal values of this eigenfunction are only attained on the boundary of the triangle" [24]. Indeed, [16, Proposition 3.1 proved that the hot spots problem and the high spots problem are equivalent for an upright cylindrical tank in the absence of surface tension. In two dimensions, the high spot is located on $\partial \mathcal{F}$ for any \mathcal{B} that can be written as a negative C^2 function on \mathcal{F} such that \mathcal{B} is not tangent to \mathcal{F} at their common endpoints [16]. This result extends to three dimensions when considering the previously described two-dimensional container as the cross section of a finite canal [17]. For a radially symmetric, convex, bounded container such that \mathcal{D} is contained in the upright cylinder $\mathcal{F} \times (-\infty, 0)$, the high spot is located on $\partial \mathcal{F}$ [18]. Concerning the IFP, it is known that the high spot is located in the interior of \mathcal{F} when \mathcal{F} is either a circular hole or an infinite parallel strip [16]. All these results rely on the property that ξ_1 is proportional to the trace of the fundamental sloshing mode Φ_1 on $\overline{\mathcal{F}}$ when the fluid oscillates freely with the fundamental sloshing frequency. Finally, it was conjectured that, for a bounded planar domain with smooth \mathcal{B} such that at least one angle between \mathcal{B} and \mathcal{F} is greater than $\pi/2$, the high spot is located in the interior of \mathcal{F} [16].

- 1.2. Main results. In this paper, we investigate how the presence of surface tension affects the location of the high spot for the IFP, focusing on an infinite parallel strip and a circular hole. We use computational tools to demonstrate that the high spot is in the interior of \mathcal{F} for large Bo, but for sufficiently small Bo the high spot is on $\partial \mathcal{F}$. We plot the location of the high spot on the x-axis for an infinite parallel strip in Figure 2(a) and a circular hole in Figure 2(b) for varying Bo. The fundamental sloshing profiles for Bo $\in \{1, 20, 100\}$ are shown in Figure 2(c). In both cases, we observe that, as Bo increases, the high spot moves from the boundary of $\mathcal F$ to the interior of \mathcal{F} . This transition happens at Bo* = 8.98461 for the infinite parallel strip and at $Bo^* = 4.63462$ for the circular hole. The vertical asymptote corresponds to the high spot location for Bo $\to \infty$, i.e., in the absence of surface tension. To obtain these results we reduce the three-dimensional problem to a one-dimensional integrodifferential equation. This one-dimensional problem is then solved approximately in orthogonal polynomial spaces, specifically Legendre polynomials for the infinite parallel strip and radial polynomials for the circular hole, resulting in a generalized eigenvalue problem for sloshing frequencies. For the circular hole, the critical value Bo* is obtained by finding the value of Bo at which the concavity of the sloshing profile on $\partial \mathcal{F}$ switches from positive to negative. We show that this condition can be reformulated as a fixed point problem, yielding a precise value of Bo*.
- **1.3. Outline.** This paper is structured as follows: In section 2, we describe the derivation of the IFP with surface tension and an equivalent Fredholm integro-

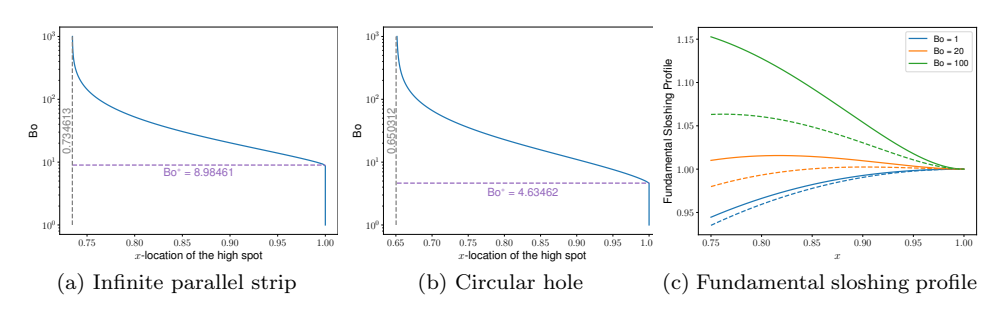


Fig. 2. Plot of the location of the high spot for (a) an infinite parallel strip and (b) a circular hole for varying Bo. The location of the high spot for the limiting case $Bo \to \infty$ is marked with a vertical asymptote. (c) The fundamental sloshing profiles near the boundary x=1 for both the infinite parallel strip (dashed lines) and the circular hole (solid lines) for $Bo \in \{1, 20, 100\}$.

differential equation. In sections 3 and 4, we describe the reduction of this equation when the aperture is an infinite parallel strip and a circular hole, respectively. In each section, we start by writing out the specific integro-differential equation before deriving the associated weak form. The weak form is numerically solved in a Legendre polynomial space in subsection 3.1 and in a radial polynomial space in subsection 4.1, yielding a generalized eigenvalue problem. Examples of sloshing profiles and frequencies as well as convergence of the numerical schemes are presented in subsections 3.2 and 4.2. In section 5, we provide a justification for the location of high spots for a circular hole that is based on determining the concavity of the sloshing profile at $\partial \mathcal{F}$. This justification depends on the numerical results but is intended to provide a basis for future analytical work on this point. We conclude in section 6 with a discussion.

2. Model derivation. The IFP can be described as the limiting case of the linear sloshing problem in a bounded domain with identical aperture; see [26, Appendix A for a detailed derivation of the linear sloshing problem with surface tension on a bounded domain. We choose the halfwidth of the equilibrium free surface \mathcal{F} as the characteristic length scale ℓ_c and nondimensionalize all lengths by ℓ_c , time by $t_c := \sqrt{\ell_c/g}$, and velocity by ℓ_c/t_c . Let $\mathbf{x} = (x, y, z)$ be dimensionless Cartesian coordinates such that the z-axis is directed vertically upward, perpendicular to the ice sheet. Let $\Phi(\mathbf{x})$ be the velocity potential with a time-harmonic factor $\cos(\omega t)$ removed and $\xi(x,y)$ be the sloshing profile, i.e., the free surface displacement, with a time-harmonic factor $\sin(\omega t)$ removed, where ω is the natural sloshing frequency. Then, the IFP with Neumann boundary conditions is a dimensionless linear boundary spectral problem for (ω, Φ, ξ) defined by

(2.1a)
$$\Delta \Phi = 0 \quad \text{in} \quad \mathcal{D} = \left\{ \mathbf{x} \in \mathbb{R}^3 : z < 0 \right\},$$

(2.1b)
$$\partial_z \Phi = 0$$
 on \mathcal{B} ,

(2.1c)
$$\partial_z \Phi = \omega \xi$$
 on \mathcal{F} ,

(2.1d)
$$\xi - \frac{1}{\text{Bo}} \Delta_{\mathcal{F}} \xi = \omega \Phi \quad \text{on} \quad \mathcal{F},$$
(2.1e)
$$\partial_{\mathbf{\hat{n}}_{\mathcal{F}}} \xi = 0 \quad \text{on} \quad \partial \mathcal{F}$$

(2.1e)
$$\partial_{\mathbf{\hat{n}}_{\mathcal{F}}}\xi = 0$$
 on $\partial \mathcal{F}$,

$$(2.1f) \qquad \int_{\mathcal{F}} \xi \, dA = 0.$$

Here, $\Delta_{\mathcal{F}}$ is the Laplacian operator on \mathcal{F} , and $\partial_{\hat{\mathbf{n}}_{\mathcal{F}}}$ is the derivative in the direction normal to $\partial \mathcal{F}$ in the plane z = 0. The two cases we consider are as follows:

Infinite parallel strip			Circular hole		
$\overline{\mathcal{F}}$	=	$\{ \mathbf{x} \in \mathbb{R}^3 \colon x < 1, z = 0 \}$	\mathcal{F}	=	${\mathbf x} \in \mathbb{R}^3 \colon (x,y) < 1, z = 0$
${\cal B}$	=	$\{\mathbf{x} \in \mathbb{R}^3 \colon x > 1, z = 0\}$	\mathcal{B}	=	$\{\mathbf{x} \in \mathbb{R}^3 \colon (x,y) > 1, z = 0\}$
$\partial \mathcal{F}$	=	$\left\{ \mathbf{x} \in \mathbb{R}^3 \colon x = 1, z = 0 \right\}$	$\partial \mathcal{F}$	=	$\left\{ \mathbf{x} \in \mathbb{R}^3 \colon (x,y) = 1, z = 0 \right\}$

The boundary condition (2.1e) is necessary as surface tension introduces the linearized curvature term $\Delta_{\mathcal{F}}\xi$ into the model. It is known as the *contact line boundary condition*, and it prescribes how the free surface moves along the container wall. In this paper we consider the *free-end edge constraint* $\partial_{\mathbf{\hat{n}}_{\mathcal{F}}}\xi = 0$ on $\partial \mathcal{F}$.

Remark 2.1. For (ω, Φ, ξ) satisfying (2.1), we have that (2.1f) additionally gives no flow at infinity, i.e., $|\nabla \Phi| \to 0$ as $|\mathbf{x}| \to \infty$. This result was shown in [10] by expanding the kernel of the solution operator in spherical harmonics.

We solve (2.1) by first expressing Φ as an integral operator acting on the Neumann boundary data $\omega\xi$, satisfying (2.1a)–(2.1c). We then plug this expression for Φ into (2.1d) to derive an equivalent eigenvalue integro-differential equation for (ω^2, ξ) . We start by considering the Laplace problem with compactly supported Neumann data:

(2.2a)
$$\Delta\Phi(\mathbf{x}) = 0 \quad \text{in} \quad \mathcal{D} = \left\{ \mathbf{x} \in \mathbb{R}^3 : z < 0 \right\},$$

(2.2b)
$$\partial_z \Phi(\mathbf{x}) = f(\mathbf{x}) \chi_{\mathcal{F}}(\mathbf{x}) \text{ on } \partial \mathcal{D} = \left\{ \mathbf{x} \in \mathbb{R}^3 : z = 0 \right\}.$$

Remark 2.2. By defining $f = \omega \xi$ it is easy to see that (2.1f) is the compatibility condition $\int_{\partial \mathcal{D}} f \, d\mathbf{x} = 0$, guaranteeing the existence and uniqueness up to a constant, of the Neumann problem for Φ in the half-space.

Remark 2.3. If (ω, Φ, ξ) is a solution of (2.1), then so are $(\omega, -\Phi, -\xi)$, $(-\omega, -\Phi, \xi)$, and $(-\omega, \Phi, -\xi)$. There is no contradiction with the previous remark, as for a given (ω, ξ) pair, Φ is unique up to a constant.

DEFINITION 2.4. Let S be the operator such that $\Phi(\mathbf{x})$ satisfying (2.2) can be written as $\Phi(\mathbf{x}) = S[f\chi_{\mathcal{F}}](\mathbf{x}) + \Phi_{\infty}$, where Φ_{∞} is constant and $Sf(\mathbf{x}) \to 0$ as $|\mathbf{x}| \to \infty$.

Examples of S for an infinite parallel strip and a circular hole are given in sections 3 and 4, respectively. Comparing (2.2b) and (2.1b)–(2.1c), we set $f = \omega \xi$ and plug in (2.1d). This gives the following equation on the free surface:

(2.3)
$$\xi - \frac{1}{\text{Bo}} \Delta_{\mathcal{F}} \xi = \omega^2 \hat{S} \xi + \omega \Phi_{\infty}.$$

Here \widehat{S} is the restriction of S to the free surface \mathcal{F} . To remove Φ from this equation entirely, resulting in an eigenvalue integro-differential equation for (ω^2, ξ) , we utilize (2.1f). Motivated by [10], we define the mean value operator to be $Mf = \frac{1}{|\mathcal{F}|} \int_{\mathcal{F}} f \, dA$, and next we consider (I - M), where I is the identity operator. Note that (I - M) applied to a constant yields 0 and $(I - M)\xi = \xi$. Therefore, applying (I - M) to (2.3) and including the appropriate conditions on ξ yield

(2.4a)
$$\xi - \frac{1}{\text{Bo}}(I - M)\Delta_{\mathcal{F}}\xi = \omega^2(I - M)\widehat{S}\xi \quad \text{on} \quad \mathcal{F},$$

(2.4b)
$$\partial_{\hat{\mathbf{n}}_{\mathcal{F}}} \xi = 0$$
 on $\partial \mathcal{F}$

together with $\int_{\mathcal{F}} \xi \, dA = 0$. The following theorem establishes equivalence between solutions of (2.1) and (2.4).

THEOREM 2.5. Let S be as in Definition 2.4 with $f = \omega \xi$. If (ω, Φ, ξ) is a solution to (2.1), then (ω^2, ξ) solves (2.4). Moreover, if (ω^2, ξ) is a solution to (2.4) and we define $\Phi = \omega S \xi - \omega M \hat{S} \xi - \frac{1}{\omega Bo} M \Delta_{\mathcal{F}} \xi$, then (ω, Φ, ξ) is a solution to (2.1).

Proof. The first statement is a direct result of the derivation of (2.4) along with Remark 2.2. The second statement follows from the facts that $\omega M \hat{S} \xi$ and $\frac{1}{\omega \text{Bo}} M \Delta_{\mathcal{F}} \xi$ are constant and therefore (2.1a)–(2.1c) are trivially satisfied due to the operator S. Restricting the definition of Φ to the free surface, we have $\Phi = \omega (I - M) \hat{S} \xi - \frac{1}{\omega \text{Bo}} M \Delta_{\mathcal{F}} \xi$. Therefore, from (2.4a) we find

$$\omega \Phi = \xi - \frac{1}{\text{Bo}} (I - M) \Delta_{\mathcal{F}} \xi - \frac{1}{\text{Bo}} M \Delta_{\mathcal{F}} \xi$$
 on \mathcal{F}

such that (ω, Φ, ξ) satisfies (2.1d).

In the case of an infinite parallel strip, we show in section 3 that (2.4) with $\int_{\mathcal{F}} \xi \, dA = 0$ has an infinite sequence of positive eigenvalues $\{\omega_n^2\}_{n=1}^{\infty}$.

3. Infinite parallel strip. In the case of an infinite parallel strip, we assume no dependence on y and therefore consider a cross section as in Figure 1. Using [10, 32], we have the following representation of bounded solutions to the Neumann problem.

LEMMA 3.1. In the case of an infinite parallel strip with $\Phi(\mathbf{x}) = \Phi(x, z)$, there exists a bounded solution to (2.2) of the form $\Phi(x, z) = S[f\chi_{[-1,1]}](x,z) + \Phi_{\infty}$, where

$$S[f\chi_{[-1,1]}](x,z) = -\frac{1}{2\pi} \int_{-1}^{1} \ln\left((x-s)^2 + z^2\right) f(s) \, ds, \quad \Phi_{\infty} = \lim_{|(x,z)| \to \infty} \Phi(x,z).$$

Proof. The existence up to a constant follows from the compatibility condition. Since $Sf(x,z) \to 0$ as $|(x,z)| \to \infty$ [29], the constant is $\Phi_{\infty} = \lim_{|(x,z)| \to \infty} \Phi(x,z)$. The fact that Φ satisfies (2.2) and that Φ is bounded can be found in [32].

Lemma 3.1 gives the form of S as in Definition 2.4 with restriction to z=0 given by $\widehat{S}\xi(x)=-\frac{1}{\pi}\int_{-1}^{1}\ln|x-s|\xi(s)\,ds$. Therefore, using Theorem 2.5, plugging into (2.4), and keeping in mind that $\Phi(\mathbf{x})=\Phi(x,z)$, we are seeking solutions (ω^2,ξ) of the following eigenvalue integro-differential equation:

(3.1a)
$$\xi - \frac{1}{B_0} (I - M) \xi'' = \omega^2 (I - M) \widehat{S} \xi \quad \text{on } (-1, 1),$$

(3.1b)
$$\xi'(\pm 1) = 0, \qquad \int_{-1}^{1} \xi \, dx = 0.$$

We first show that (3.1) has a discrete spectrum.

THEOREM 3.2. Define the Hilbert space $H = \{\xi \in L^2(-1,1) : \int_{-1}^1 \xi \, dx = 0\}$ with the standard L^2 -norm. The infinite parallel strip IFP (3.1) has a discrete sequence of positive eigenvalues $\{\omega_n^2\}_{n=1}^{\infty}$,

$$0 < \omega_1^2 \le \omega_2^2 \le \dots \to \infty,$$

and the corresponding eigenfunctions $\{\xi_n\}_{n=1}^{\infty}$ belong to H.

Proof. Define the operator \mathcal{P} by $\mathcal{P}\xi \coloneqq \xi - \frac{1}{\mathrm{Bo}}(I - M)\xi''$ with domain $D(\mathcal{P}) = \{\xi \in H^2(-1,1) \cap H \colon \xi'(\pm 1) = 0\}$. Testing (3.1a) with $\xi \in D(\mathcal{P})$, we see that \mathcal{P} is symmetric. Moreover, the Poincaré–Wirtinger inequality gives $\|\mathcal{P}\xi\|_H \geq C\|\xi\|_H^2$ for some constant C > 0. It follows that \mathcal{P} admits a self-adjoint Friedrichs extension which we denote by \mathcal{P} again. Furthermore, it was shown that \widehat{S} and thus $(I - M)\widehat{S}$ are self-adjoint, positive definite, and compact on H [10, Lemmas 5, 6, 7]. The desired result then follows from [14, subsection 1.4.2].

We now turn our attention to seeking weak eigenpairs of (3.1). Define the Hilbert space $V = \{\xi \in H^2(-1,1) : \xi'(\pm 1) = 0, \int_{-1}^1 \xi \, dx = 0\}.$

DEFINITION 3.3. We say that $(\omega^2, \xi) \in \mathbb{R} \times V$ is a weak sloshing eigenpair of (3.1) if the following holds for all $g \in V$:

(3.2)
$$\int_{-1}^{1} \left(\xi g + \frac{1}{\text{Bo}} \xi' g' \right) dx = -\frac{\omega^2}{\pi} \int_{-1}^{1} \int_{-1}^{1} \ln|x - s| \xi(s) g(x) \, ds dx.$$

(3.2) is formally obtained by multiplying (3.1a) by g, integrating from -1 to 1, using integration by parts with the prescribed boundary conditions, and simplifying with the fact that $M\xi''$ and $M\hat{S}\xi$ are constant and $\int_{-1}^{1} g \, dx = 0$.

3.1. Polynomial approximation. We seek approximate solutions to (3.2) in a finite-dimensional polynomial space. Let p_j denote the normalized Legendre polynomial of degree $j \geq 0$ on [-1,1] with respect to the weight 1, i.e., $\int_{-1}^{1} p_j p_k dx = \delta_{jk}$. Following [25], we define the spaces $P^{(n)} = \text{span} \{p_0(x), p_1(x), \dots, p_n(x)\}$ and $W^{(n)} = \{v \in P^{(n)}: v'(\pm 1) = 0, \int_{-1}^{1} v dx = 0\}$. Suppose (ω^2, ξ) is a weak sloshing eigenpair of the infinite parallel strip IFP, as in Definition 3.3, and let $\xi^{(n)}$ be the orthogonal projection of ξ to $W^{(n)}$ with respect to the $L^2(-1,1)$ inner product. In general [3, equation 9.4.10] we have

$$\left\| \xi - \xi^{(n)} \right\|_{H^{\ell}(-1,1)} \le C n^{-1/2} n^{2\ell - m} \|\xi\|_{H^m(-1,1)}$$

for $\xi \in H^m(-1,1)$ with $1 \le \ell \le m$. In particular, since $\xi \in V \subset H^2(-1,1)$, we have the a priori convergence result that $\xi^{(n)} \to \xi$ in $H^1(-1,1)$ as $n \to \infty$. Furthermore, the convergence will be faster if ξ is more regular and, in practice, we observe a higher rate of convergence; see subsection 3.2.

For every $j=1,2,\ldots$, define the polynomial $q_j=(p_j-\beta_jp_{j+2})/\alpha_j$, which trivially satisfies $\int_{-1}^1 q_j \, dx=0$ due to the orthogonality of the Legendre polynomials p_j . We choose $\beta_j=\frac{j(j+1)\sqrt{2j+1}}{(j+2)(j+3)\sqrt{2j+5}}$ and $\alpha_j=\sqrt{1+\beta_j^2}$ to satisfy the Neumann boundary conditions and to normalize q_j such that $\int_{-1}^1 q_j^2 \, dx=1$, respectively.

LEMMA 3.4. The set of polynomials $\{q_j\}_{j=1}^{n-2}$ for $n=3,4,\ldots$ constitutes a basis for $W^{(n)}$.

Proof. The statement follows from [25, 1].

Therefore, the discrete weak formulation of the infinite parallel strip IFP is to find $(\omega^2, \xi^{(n)}) \in \mathbb{R} \times W^{(n)}$ such that for all $g \in W^{(n)}$ we have

(3.3)
$$\int_{-1}^{1} \left(\xi^{(n)} g + \frac{1}{\text{Bo}} \left(\xi^{(n)} \right)' g' \right) dx = -\frac{\omega^2}{\pi} \int_{-1}^{1} \int_{-1}^{1} \ln|x - s| \xi^{(n)}(s) g(x) ds dx.$$

THEOREM 3.5. If $(\omega^2, \xi^{(n)}) \in \mathbb{R} \times W^{(n)}$ solves the discrete infinite parallel strip IFP (3.3), then $(\omega^2, \xi^{(n)})$, with $\xi^{(n)} = \sum_{j=1}^{n-2} c_j q_j$, solves the following generalized eigenvalue problem for $i = 1, 2, \ldots, n-2$:

(3.4)
$$\sum_{j=1}^{n-2} c_j \left(M_{ij} + \frac{1}{\text{Bo}} K_{ij} \right) = \omega^2 \sum_{j=1}^{n-2} c_j L_{ij}.$$

Here, $M_{ij} = \int_{-1}^{1} q_i(x) q_j(x) dx$ is the mass matrix, $K_{ij} = \int_{-1}^{1} q_i'(x) q_j'(x) dx$ is the stiffness matrix, and $L_{ij} = -\int_{-1}^{1} \int_{-1}^{1} \ln|x - s| q_i(x) q_j(s) ds dx$, which are given by

$$\begin{split} M_{ij} &= \delta_{ij} - \frac{\beta_i}{\alpha_i \alpha_{i+2}} \delta_{i+2,j} - \frac{\beta_{i-2}}{\alpha_{i-2} \alpha_i} \delta_{i-2,j}, \\ K_{ij} &= \frac{\beta_j \sqrt{2j+5}}{\alpha_j^2 \sqrt{2j+1}} (2j+1)(2j+3) \delta_{ij}, \\ L_{ij} &= \frac{-\tilde{L}_{ij} + \beta_i \tilde{L}_{i+2,j} + \beta_j \tilde{L}_{i,j+2} - \beta_i \beta_j \tilde{L}_{i+2,j+2}}{\alpha_i \alpha_j}, \\ \tilde{L}_{ij} &= \begin{cases} \frac{4}{\pi} \frac{\sqrt{2i+1} \sqrt{2j+1}}{(i+j)(i+j+2)(1-(i-j)^2)} & \text{if } i+j \text{ is even,} \\ 0 & \text{otherwise.} \end{cases} \end{split}$$

Proof. Choosing $g = q_i$ in (3.3), expanding the q_i and q_j polynomials, and using [5], we find the expression for L_{ij} . To compute M_{ij} and K_{ij} , it suffices to consider the case where $i \leq j$ since they are symmetric expressions. Using orthonormality of the Legendre polynomials, p_i , the expression for M_{ij} follows. To obtain K_{ij} , we integrate by parts and use the fact that $q'_i(\pm 1) = 0$ for $W^{(n)}$ to get

$$K_{ij} = -\frac{1}{\alpha_j} \left[\int_{-1}^1 q_i'' p_j \, dx - \beta_m \int_{-1}^1 q_i'' p_{j+2} \, dx \right].$$

Since q_i'' is at most degree i and the Legendre polynomial p_j is orthogonal to any polynomial of lower degree, we see that $K_{ij} = 0$ if i < j and

$$K_{jj} = \frac{\beta_j}{\alpha_j^2} \int_{-1}^1 p_{j+2}'' p_j \, dx = \frac{\beta_j \sqrt{2j+5}}{\alpha_j^2 \sqrt{2j+1}} (2j+1)(2j+3).$$

The final value for K_{jj} follows from the orthonormality of the Legendre polynomials, p_j , together with the well-known relationship,

$$p_j''(x) = \sqrt{2j+1} \sum_{\substack{k=0\\k+j \text{ even}}}^{j-2} \left(k + \frac{1}{2}\right) \left(j(j+1) - k(k+1)\right) \frac{p_k(x)}{\sqrt{2k+1}}.$$

We note that a benefit of our choice of basis to strongly enforce the Neumann boundary conditions, as opposed to weakly enforcing it, is that all of the boundary information is encoded in the β_j . Therefore, it is easy to generalize the work presented here to other boundary conditions. For example, if homogeneous Dirichlet boundary conditions were considered, we instead define $\beta_j = \frac{2j+1}{2j+5}$.

Table 1 The first three eigenvalues for the infinite parallel strip IFP for $Bo \in \{1, 10, 50, \infty\}$.

	Bo = 1	Bo = 10	Bo = 50	$Bo = \infty$
j=1	7.0326	2.5238	2.1162	2.0061
j=2	37.7871	6.9032	4.1530	3.4533
j=3	119.0961	16.5480	7.4307	5.1253

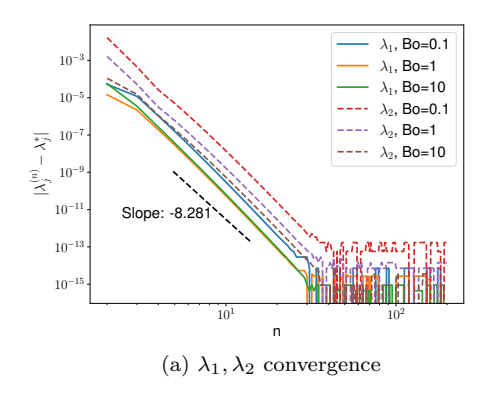
3.2. Numerical results. We now solve (3.4), which is a generalized eigenvalue problem of the form

(3.5)
$$\left(\mathbf{M} + \frac{1}{\mathrm{Bo}}\mathbf{K}\right)\boldsymbol{\xi} = \lambda \mathbf{L}\boldsymbol{\xi}, \quad \lambda := \omega^2,$$

where $(\boldsymbol{\xi})_i = c_i$ and \mathbf{M} , \mathbf{K} , \mathbf{L} are square matrices. The mass matrix \mathbf{M} is pentadiagonal, the stiffness matrix \mathbf{K} is diagonal, and the matrix \mathbf{L} is dense but exhibits a checkerboard pattern as $L_{ij} = 0$ if i+j is odd. Specifically, the only nonzero diagonals for \mathbf{M} are the main diagonal and the second sub- and superdiagonals. It follows from Theorem 2.5 that the eigenvalues λ_j of (3.5) approximate the first n of the natural sloshing frequencies of IFP squared.

The first three eigenvalues of (3.5) for $Bo \in \{1, 10, 50, \infty\}$ with n = 200 are shown in Table 1. To validate our solution to the infinite parallel strip IFP for $Bo = \infty$, we compare the eigenvalues to those found in Fox and Kuttler [8] and found that for all eigenvalues reported our results fit within the bounds provided. A table of all previous results [10, 5, 20] is given in [8], and it is the case that Fox and Kuttler provide the tightest bounds among the zero surface tension results. To get an understanding of the surface tension effects on the fundamental sloshing frequency we note that $\frac{\lambda_1(Bo=1)}{\lambda_1(Bo=\infty)} = 3.506$. That is, when the force due to surface tension is comparable to the gravitational force the fundamental sloshing frequency is increased to more than 300% of the value when surface tension is negligible.

Figure 3(a) illustrates the convergence plots of the first two sloshing frequencies, i.e., j=1,2, and their corresponding sloshing profiles in Figure 3(b) for Bo $\in \{0.1,1,10\}$. The true solution (λ_j^*,ξ_j^*) is the highly resolved (n=2000) solution from our method. We observe high rates of convergence for finite Bo for both the sloshing



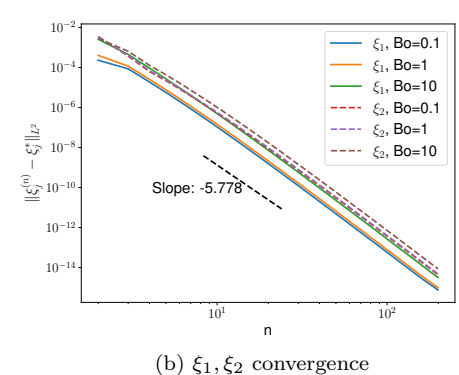


Fig. 3. Log-log convergence plots of the first (solid) and second (dashed) eigenvalues and their corresponding sloshing profiles for $Bo \in \{0.1, 1, 10\}$. The true solution is approximated with n = 2000.

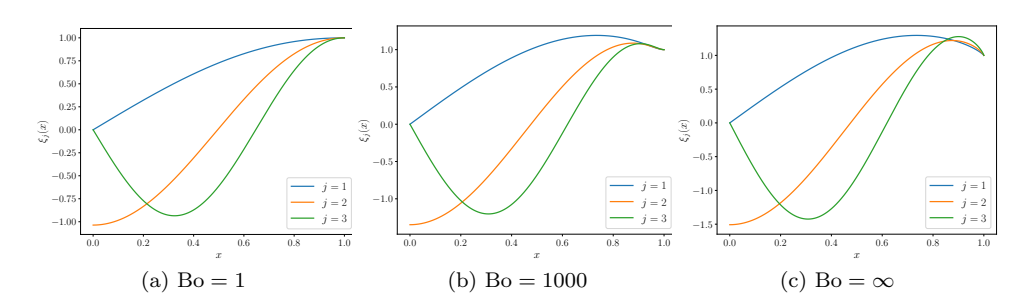


FIG. 4. The first three sloshing profiles for the infinite parallel strip IFP for Bo $\in \{1, 1000, \infty\}$. Even though $\xi(x)$ is defined on [-1, 1], solutions are only plotted on [0, 1] since $\xi(x)$ is either even or odd.

frequencies and the sloshing profiles. We note that the observed rate of convergence for $\xi^{(n)} \to \xi$ is much higher than the a priori estimate as discussed above.

The first three sloshing profiles for j=1,2,3 are shown in Figure 4 for Bo = 1 in Figure 4(a), for Bo = 1000 in Figure 4(b), and for Bo = ∞ corresponding to the zero surface tension case in Figure 4(c). The sloshing profiles for the infinite parallel strip IFP appear to be unchanged for Bo < 10. Most interesting is the behavior of the high spot of the fundamental sloshing profile for moderate Bo. This will be further discussed in section 5; here we simply note that for small Bo the high spot is located on $\partial \mathcal{F}$, whereas for large Bo the high spot has moved to the interior of \mathcal{F} . This phenomenon is further demonstrated for Bo $\in [10^0, 10^3]$ in Figure 2(a).

4. Circular hole. For a circular hole, the outward normal to \mathcal{F} in the plane z=0 is in the radial direction. In this case, we transform the equations into cylindrical coordinates along the z-axis, and we look for azimuthal solutions. To construct the integral operator S, we consider (2.2) in cylindrical coordinates with $f(r,\theta)=f_m(r)\cos(m\theta)$. Therefore, we make the ansatz $\Phi(r,\theta,z)=\Phi_m(r,z)\cos(m\theta)$ for $m\geq 0$ with the conditions that $\Phi_0(0,z)$ is bounded and that $\Phi_m(0,z)=0$ for $m\geq 1$. Plugging the ansatz into (2.2) and canceling $\cos(m\theta)$ yield

(4.1a)
$$\Delta_m \Phi_m + \partial_{zz} \Phi_m = 0 \quad \text{in} \quad \mathcal{D} = \left\{ (r, z) \in \mathbb{R}^2 : r \ge 0, z < 0 \right\},$$
(4.1b)
$$\partial_z \Phi_m = f_m \chi_{[0, 1)} \quad \text{on} \quad \partial \mathcal{D} = \left\{ (r, z) \in \mathbb{R}^2 : r \ge 0, z = 0 \right\}.$$

In the above, $\Delta_m = \frac{1}{r}\partial_r(r\partial_r) - \frac{m^2}{r^2}$ is the Bessel differential operator. We remark that the compatibility condition is automatically satisfied for $m \geq 1$, whereas it becomes $\int_0^1 f_0 r dr = 0$ for m = 0. Furthermore, only for m = 0 can a new solution be obtained by adding a constant to any solution due to the term $\frac{m^2}{r^2}$ in Δ_m . Motivated by [20], we proceed to construct solutions to (4.1) using the Hankel transform method. Following [23], we define the Hankel transform pair, $F_m(k) = \mathcal{H}\{f\}(k)$, as

$$F_m(k) = \int_0^\infty r f(r) J_m(kr) dr$$
 and $f(r) = \int_0^\infty k F_m(k) J_m(kr) dk$,

with J_m being the Bessel functions of the first kind. Using the fact that $\mathcal{H}\{\Delta_m f\}(k) = -k^2\mathcal{H}\{f\}(k)$ [23], (4.1a) becomes an integrable equation for $H_m = \mathcal{H}\{\Phi_m\}$. Looking for bounded solutions as $z \to -\infty$, the general solution has the form $H_m(k, z) = A(k)e^{kz}$. The constant of integration A(k) is obtained using the Neumann boundary conditions (4.1b). Rearranging reveals that $kA(k) = \mathcal{H}\{f_m\}(k)$. We note that

since $f_m(r)$ is compactly supported, the inverse Hankel transform is well defined [23]. Therefore, we have a solution to the Neumann problem.

LEMMA 4.1. For a circular hole with $f(r,\theta) = f_m(r)\cos(m\theta)$, where $\sqrt{r}f_m(r) \in L^2(0,1)$, there exists a bounded solution to (2.2) that can be represented as

$$\Phi(r,\theta,z) = \int_0^\infty \int_0^1 s f_m(s) J_m(ks) e^{kz} J_m(kr) ds dk \cos(m\theta) + c_m = Sf(r,\theta,z) + c_m,$$

with $c_m = 0$ if $m \ge 1$. Furthermore, we have $Sf(r, \theta, z) \to 0$ as $|(r, z)| \to \infty$, θ fixed.

Proof. It is straightforward to show that Φ is a solution to (4.1). Let $G(k) = \int_0^1 \sqrt{s} f_m(s) \sqrt{s} J_m(ks) ds$. Using the Cauchy–Schwarz inequality and the integral formula [22, Eq. 10.22.5] with $\mu = m$, we obtain

$$|G(k)|^2 \le \|\sqrt{s}f_m(s)\|_{L^2(0,1)}^2 \cdot \frac{1}{2} \Big[J_m^2(k) - J_{m-1}(k)J_{m+1}(k)\Big].$$

It follows that

$$||G(k)||_{L^4(0,\infty)}^4 \le ||\sqrt{s}f_m(s)||_{L^2(0,1)}^4 \int_0^\infty \left[J_m^4(k) + J_{m-1}^2(k)J_{m+1}^2(k)\right]dk < \infty$$

since $J_m(k)$ is continuous on $[0,\infty)$ and $|J_m(k)| \le k^{-1/3}$ for all k [19]. Thus $G(k) \in L^4(0,\infty)$. Next, using Hölder's inequality with p=4 and q=p/(p-1)=4/3, we obtain

$$|Sf| \le \int_0^\infty |G(k)e^{kz}J_m(kr)| dk \le ||G(k)||_{L^4(0,\infty)} ||e^{kz}J_m(kr)||_{L^{4/3}(0,\infty)}.$$

To estimate the second term on the right, we use the same bound as above on $|J_m(k)|$ and a change of variables. We have

$$\left\| e^{kz} J_m(kr) \right\|_{L^{4/3}(0,\infty)}^{4/3} \le \int_0^\infty \frac{e^{4kz/3}}{(kr)^{4/9}} \, dk = \left(\frac{3}{4}\right)^{5/9} \frac{1}{(-z)^{5/9} r^{4/9}} \Gamma(5/9),$$

where $\Gamma(u)$ is the gamma function. Since the last expression on the right goes to zero as $r^2 + z^2 \to \infty$ with r > 0 and z < 0, the claim follows.

Considering the form of the surface equation (2.1d) for ξ in cylindrical coordinates and looking for azimuthal solutions, we make the same ansatz $\xi(r,\theta) = \xi_m(r)\cos(m\theta)$. Therefore, for each $m \geq 0$, Lemma 4.1 gives the form of the integral operator S defined in Definition 2.4 with the restriction to z = 0 given by

$$\widehat{S}\xi(r,\theta) = \int_0^\infty \int_0^1 s\xi_m(s)J_m(ks)J_m(kr)\,dsdk\cos(m\theta).$$

Therefore, using Theorem 2.5, plugging into (2.4a), transforming in cylindrical coordinates, using the ansatz, noting that $M(\xi_m \cos(m\theta)) = 0$ for $m \ge 1$, and canceling the cosine, we have the following eigenvalue integro-differential equation

(4.2)
$$\xi_m - \frac{1}{\text{Bo}} \Delta_m \xi_m = \omega^2 \widehat{S}_r \xi_m(r) \quad \text{for} \quad m \ge 1,$$

where $\widehat{S}_r \xi_m(r) = \int_0^\infty \int_0^1 \xi_m(s) s J_m(ks) J_m(kr) ds dk$ is the radial part of \widehat{S} . In the case m=0, we recall that, from (2.1f), we require $\int_0^1 \xi_0 r dr = 0$. We have $\Phi = \Phi_0(r,z)$ and $\xi = \xi_0(r)$ so that the application of Theorem 2.5 in cylindrical coordinates yields

(4.3)
$$\xi_0 - \frac{1}{\text{Bo}}(I - M) \left(\frac{1}{r}(r\xi_0')'\right) = \omega^2(I - M)\widehat{S}_r\xi_0(r) \quad \text{for} \quad m = 0.$$

The boundary conditions to (4.2)–(4.3) are $\xi'_m(1) = 0$, $\xi_0(0)$ bounded and $\xi_m(0) = 0$ for $m \ge 1$.

We now look for weak eigenpairs to (4.2) and (4.3). Define the Hilbert spaces

$$V_0 = \left\{ \xi_0 \in H_r^2(0,1) : \xi_0'(1) = 0, \xi_0(0) \text{ is bounded, } \int_0^1 r \xi_0 \, dr = 0 \right\}$$

$$V_m = \left\{ \xi_m \in H_r^2(0,1) : \xi_m'(1) = 0, \xi_m(0) = 0 \right\}, \qquad m \ge 1,$$

where the subscript r indicates the weighted Sobolev space with respect to the weight function w(r) = r. Consider $m \ge 1$, and let g be a test function in V_m . Multiplying (4.2) by g(r)r, integrating from 0 to 1, and using integration by parts along with the boundary conditions, we get the weak formulation

(4.4)
$$\int_0^1 \left(\xi_m g r + \frac{1}{\text{Bo}} \frac{m^2}{r} \xi_m g + \frac{1}{\text{Bo}} \xi'_m g' r \right) dr = \omega^2 \int_0^1 \widehat{S}_r \xi_m(r) g(r) r \, dr, \quad m \ge 1.$$

Consider m = 0, and again let g be a test function in V_0 . Multiplying (4.3) by g(r)r, integrating from 0 to 1, using integration by parts along with the boundary conditions, and remembering that the M operator produces a constant, we find the weak formulation

(4.5)
$$\int_0^1 \left(\xi_0 g r + \frac{1}{\text{Bo}} \xi_0' g' r \right) dr = \omega^2 \int_0^1 \widehat{S}_r \xi_0(r) g(r) r \, dr.$$

It is obvious that (4.4) and (4.5) can be reformulated as a single weak formulation.

DEFINITION 4.2. We say that $(\omega^2, \xi_m) \in \mathbb{R} \times V_m$ is a weak sloshing eigenpair of (4.2), or (4.3) when m = 0, if the following holds for all $g \in V_m$ for $m \geq 0$:

(4.6)
$$\int_0^1 \left(\xi_m g r + \frac{1}{\text{Bo}} \frac{m^2}{r} \xi_m g + \frac{1}{\text{Bo}} \xi'_m g' r \right) dr = \omega^2 \int_0^1 \widehat{S}_r \xi_m(r) g(r) r \, dr.$$

4.1. Polynomial approximation. We look for approximate solutions to (4.6) in a finite-dimensional space. From the Hankel representation $\int_0^\infty k^2 A(k) J_m(kr) dk = f_m(r)$ with $f_m(r) = \omega \xi_m(r)$ along with the fact that $J_m(r) \sim \frac{r^m}{2^m \Gamma(m+1)}$ as $r \to 0$ [22, Eq. 10.7.3] we note that it is therefore necessary that $f_m(r) = O(r^m)$ as $r \to 0$. This fact motivates the use of the radial polynomials $h_j^m(r) = \mu_j^m r^m p_{j-1}^{(0,m)}(2r^2 - 1)$, with $p_j^{(\alpha,\beta)}(x)$ being the Jacobi polynomials and $\mu_j^m = 2\sqrt{j+\frac{1}{2}(m-1)}$. We note that these polynomials are orthogonal on (0,1) with respect to the weight function r, i.e., $\int_0^1 h_i^m(r) h_j^m(r) r dr = \delta_{ij}$. This fact follows simply from a change of variables, the orthogonality of Jacobi polynomials, and the fact that [22, Eq. 18.3.1] $\int_{-1}^1 (1+x)^m (p_{j-1}^{(0,m)}(x))^2 dx = \frac{2^{m+1}}{2i+m-1}$. Moreover, we note that $\int_0^1 h_j^0 r \, dr = 0$ for $j = 2, 3, \ldots$ Now we define $P_m^{(n)} = \operatorname{span}\{h_1^m(x), \ldots, h_n^m(x)\}$ same as the infinite parallel strip and analogously define

$$W_m^{(n)} = \left\{ v \in P_m^{(n)} \colon v'(1) = 0 \text{ and } \int_0^1 vr \, dr = 0 \text{ if } m = 0 \right\}.$$

LEMMA 4.3. Suppose (ω^2, ξ_m) is a weak sloshing eigenpair of the circular hole IFP, as in Definition 4.2, and let $\xi_m^{(n)}$ be the orthogonal projection of ξ_m to $W_m^{(n)}$

with respect to the $L_r^2(0,1)$ inner product. When $m \geq 1$, if $\xi_m \in V_m \subset H_r^2(0,1)$ and $\frac{\xi_m}{r} \in L_r^2(0,1), \ then$

$$\left\| \xi_m - \xi_m^{(n)} \right\|_{L_r^2(0,1)} \le C n^{-1} \left(m \left\| \frac{\xi_m(r)}{r} \right\|_{L_r^2(0,1)} + \|\xi_m'(r)\|_{L_r^2(0,1)} \right),$$

where the constant C is independent of n.

Remark 4.4. The result holds for m=0 simply if $\xi_0 \in V_0$.

Proof. We denote the space of L^2 -integrable functions on (-1,1) with respect to the Jacobi weight function $w(x) = (1-x)^{\alpha}(1+x)^{\beta}$ as $L^2_{\alpha,\beta}$. Now, we note that $\sum_{j=1}^{n-2} \alpha_j h_j^m$ being the orthogonal projection of $\xi_m(r)$ with respect to the $L_r^2(0,1)$ inner product is equivalent to $\sum_{j=1}^{n-2} \frac{\alpha_j \mu_j^m}{2(2^{m/2})} p_{j-1}^{(0,m)}(x)$ being the orthogonal projection of $\frac{1}{2}(\frac{1}{x+1})^{m/2}\xi_m(\sqrt{\frac{x+1}{2}})$ with respect to the $L^2_{0,m}$ inner product. Then, by a change of variables and [9, Theorem 2.1] we have that

$$\begin{split} \left\| \xi_m - \xi_m^{(n)} \right\|_{L_r^2(0,1)} &= \left\| \frac{1}{2} \left(\frac{1}{x+1} \right)^{m/2} \xi_m \left(\sqrt{\frac{x+1}{2}} \right) - \sum_{j=1}^{n-2} \frac{\alpha_j \mu_j^m}{2(2^{m/2})} p_{j-1}^{(0,m)}(x) \right\|_{L_{0,m}^2} \\ &\leq C n^{-k} \left\| \frac{d^k}{dx^k} \left(\frac{1}{2} \left(\frac{1}{x+1} \right)^{m/2} \xi_m \left(\sqrt{\frac{x+1}{2}} \right) \right) \right\|_{L_x^2 - 1}. \end{split}$$

To relate back to the $L_r^2(0,1)$ inner product we consider the specific case with k=1, change variables, and use the triangle inequality to determine

$$\left\| \frac{d}{dx} \left(\frac{1}{2} \left(\frac{1}{x+1} \right)^{m/2} \xi_m \left(\sqrt{\frac{x+1}{2}} \right) \right) \right\|_{L^2_{1,m+1}} \le m \left\| \frac{\xi_m(r)}{r} \right\|_{L^2_{r}(0,1)} + \left\| \xi'_m(r) \right\|_{L^2_{r}(0,1)},$$

and the result follows.

To strongly enforce the Neumann boundary conditions, we define $q_j^m = h_j^m + \beta_j^m h_{j+1}^m$, where the constant β_j^m is such that $(q_j^m)'(1) = 0$. We know [22, Eq. 18.6.1] that $p_n^{(0,m)} = \frac{(1)_n}{n!} = 1$ and that $\frac{d}{dr} p_{j-1}^{(0,m)}(1) = \frac{(j-1)(j+m)}{2}$, which comes from evaluating the Jacobi polynomial differential equation at 1, yielding $(h_j^m)'(1) = \frac{d^m}{dr} p_j^m = \frac{d^m}{dr}$ $\mu_j^m m + 2\mu_j^m (j-1)(j+m)$. Therefore, we have that $\beta_j^m = -\frac{\mu_j^m (m+2(j-1)(j+m))}{\mu_{j+1}^m (m+2j(j+m+1))}$.

Therefore, the discrete weak formulation of the circular hole IFP (4.6) is to find

 $(\omega^2, \xi_m^{(n)}) \in \mathbb{R} \times W_m^{(n)}$ such that for all $g \in W_m^{(n)}$ we have

(4.7)
$$\int_0^1 \left(\xi_m^{(n)}(r)g(r)r + \frac{1}{\text{Bo}} \frac{m^2}{r} \xi_m^{(n)}(r)g(r) + \frac{1}{\text{Bo}} \left(\xi_m^{(n)}(r) \right)' g'(r)r \right) dr$$

$$= \omega^2 \int_0^1 \int_0^\infty \int_0^1 \xi_m^{(n)}(s) s J_m(ks) J_m(kr) g(r) r \, ds dk dr.$$

THEOREM 4.5. If $(\omega^2, \xi_m^{(n)}) \in \mathbb{R} \times W_m^{(n)}$ solves the discrete circular hole IFP (4.7), then $(\omega^2, \xi_m^{(n)})$, with $\xi_m^{(n)} = \sum_{j=1}^n a_j^m q_j^m$, solves the following generalized eigenvalue problem for $i = 1, 2, \ldots, n$:

(4.8)
$$\sum_{j=1}^{n} a_j^m \left(M_{ij}^m + \frac{1}{\text{Bo}} K_{ij}^m \right) = \omega^2 \sum_{j=1}^{n} a_j^m L_{ij}^m.$$

Here, $M_{ij}^m = \int_0^1 q_j^m q_i^m r \, dr$ is the mass matrix, $K_{ij}^m = \int_0^1 (\frac{m^2}{r} q_j^m q_i^m + (q_j^m)'(q_i^m)'r) dr$ is the stiffness matrix, and $L_{ij}^m = \int_0^1 \int_0^\infty \int_0^1 q_j^m(s) J_m(ks) s \, ds J_m(kr) \, dk q_i^m(r) r dr$. For the m=0 case, this simply needs to be edited to $\xi_m = \sum_{j=2}^n a_j^m q_j^m$, and it only holds for $i=2,3,\ldots,n$. Moreover,

$$\begin{split} M^m_{ij} &= \left(1 + (\beta^m_i)^2\right) \delta_{ij} + \beta^m_i \delta_{i+1,j} + \beta^m_{i-1} \delta_{i-1,j}, \\ K^m_{ij} &= -\mu^m_j \mu^m_{j+1} \left(\mu^{m+1}_j\right)^2 \beta^m_j \delta_{ij}, \\ L^m_{ij} &= \tilde{L}^m_{ij} + \beta^m_i \tilde{L}^m_{i+1,j} + \beta^m_j \tilde{L}^m_{i,j+1} + \beta^m_i \beta^m_j \tilde{L}^m_{i+1,j+1}, \\ \tilde{L}^m_{ij} &= \frac{\mu^m_j \mu^m_i}{4\pi \left((j+i+m-1)^2 - \frac{1}{4}\right) \left(\frac{1}{4} - (j-1)^2\right)}. \end{split}$$

Proof. Again, we choose $g = q_i^m$ in (4.6) to obtain the integral form of the matrices. The lengthy calculations to obtain the coefficients are given in Appendix A. \square

Similar to the infinite parallel strip IFP, we note that if homogeneous Dirichlet boundary conditions were instead considered, one would simply define $\beta_j^m = -\frac{\mu_j^m}{\mu_{j+1}^m}$.

4.2. Numerical results. Similar to the infinite parallel strip IFP we are left to solve a generalized eigenvalue problem of the form (3.5). In the circular hole IFP, the mass matrix \mathbf{M} is tridiagonal, the stiffness matrix \mathbf{K} is diagonal, and the matrix \mathbf{L} is dense. Again, it follows from Theorem 2.5 that the eigenvalues λ_j of (3.5) approximate the first n of the natural sloshing frequencies of IFP squared.

The first three eigenvalues, for $m \in \{0, 1, 10\}$, of (3.5) for the circular hole for Bo $\in \{1, 10, 50, \infty\}$ with n = 200 are shown in Table 2. To validate our solution to the circular hole IFP for Bo $= \infty$ we compare the eigenvalues to those found in Miles [20] for m = 0, 1, 2, 3 and note that for all eigenvalues reported our results agree to the accuracy given by Miles (6 digits). Miles [20] compared their results to that of Henrici, Troesch, and Wuytack [10] and found their results to be as accurate or more accurate. Miles [20] reported that the given results were computed with n = 16. The current work presents results with n = 64 to recover the same or better accuracy. This is necessary due to the enforcement of boundary conditions in the current work, which is not present in the Bo $= \infty$ problem and for this reason is not considered in [20]. In the circular hole problem, with m = 1 we have that $\frac{\lambda_1(\text{Bo}=1)}{\lambda_1(\text{Bo}=\infty)} = 4.510$. That is, when the force due to surface tension is comparable to the gravitational force the fundamental sloshing frequency is increased to more than 400% of the value when surface tension is negligible.

Figure 5(a) illustrates the convergence plots of the sloshing frequencies j = 1, 2 with m = 1 and the corresponding sloshing profiles in Figure 5(b) for Bo $\in \{0.1, 1, 10\}$.

Table 2 Eigenvalues j = 1, 2, 3 for the azimuthal modes $m \in \{0, 1, 10\}$ and for $Bo \in \{1, 10, 50, \infty\}$.

		Bo = 1	Bo = 10	Bo = 50	$Bo = \infty$
	j = 1	64.9935	10.2253	5.3528	4.1213
m=0	j=2	369.5505	43.5842	14.6085	7.3421
	j=3	1100.4019	119.5281	32.3396	10.5171
	j = 1	12.4245	3.7758	2.9854	2.7548
m=1	j=2	172.4077	22.5719	9.2589	5.8921
	j=3	665.6328	74.7182	22.1968	9.0329
	j = 1	1971.9593	209.8054	53.1458	13.5734
m = 10	j=2	4740.2111	489.8354	112.0301	17.4838
	j=3	8611.8754	880.1861	192.9290	21.0661

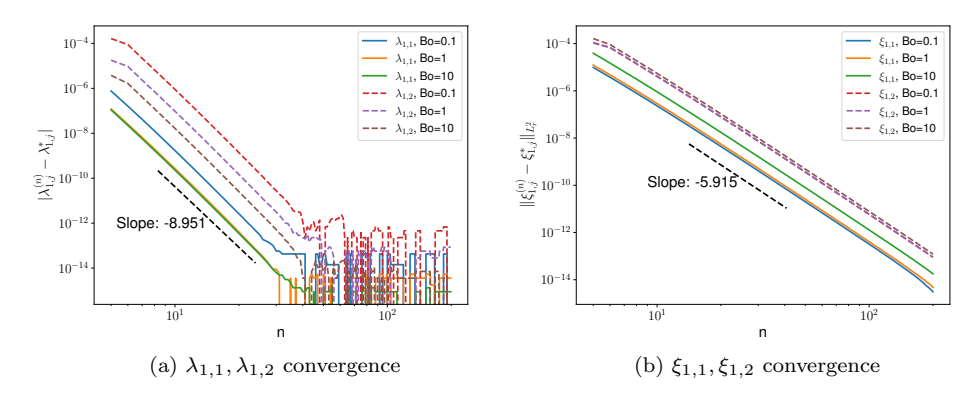


Fig. 5. Log-log convergence plots of the first (solid) and second (dashed) eigenvalues and their sloshing profiles for $Bo \in \{0.1, 1, 10\}$ with m = 1. The true solution is approximated with n = 2000.

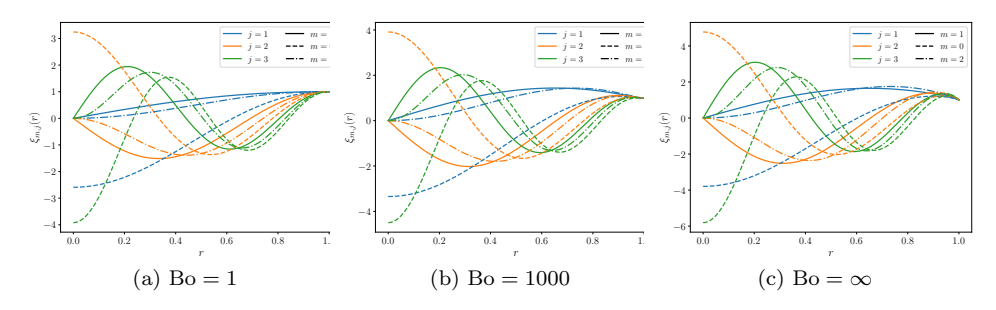


Fig. 6. The first three sloshing profiles j=1,2,3 (blue, orange, green) for the circular hole IFP for m=0 (dashed), m=1 (solid), and m=2 (dot dashed) for $Bo \in \{1,1000,\infty\}$.

The true solution (λ_j^*, ξ_j^*) is the highly resolved (n = 2000) solution from our method. Convergence for the sloshing profiles is measured in the L_r^2 -norm. In both the sloshing frequencies and sloshing profiles we observe a high rate of convergence. This rate of convergence is unaffected by the choice of m, so only the results for m = 1 are shown.

The first three sloshing profiles, for m = 0, 1, 2, for Bo $\in \{1, 1000, \infty\}$ are shown in Figure 6. Again, the sloshing profiles for the circular hole IFP appear to be unchanged for Bo < 10. We observe the same phenomenon as observed in the infinite parallel strip case that for small Bo the high spot is located on $\partial \mathcal{F}$, whereas for large Bo the high spot has moved to the interior of \mathcal{F} . This can also be seen for Bo $\in [10^0, 10^3]$ in Figure 2(b), and it will be discussed further in section 5.

5. High spot justification for a circular hole. In this section, we offer a justification for the main result that with sufficiently strong surface tension the high spot of the sloshing profile can be moved to the boundary of the free surface. We recall that previous results in the absence of surface tension, i.e., Bo $\to \infty$, showed that the high spot for a radially symmetric aperture is always in the interior of \mathcal{F} [16]. While we focus on the fundamental sloshing profile, which corresponds to m = 1, j = 1, we demonstrate that the method described below to find the critical Bo such that the high spot is on the boundary of \mathcal{F} applies for any $m \ge 1$ when such a Bo exists. Figure 2(b) plots Bo in terms of the location of the high spot for a circular

hole, m=1, and j=1. It is obtained using Newton's method for $\xi'_1(r)$, and it shows that, for Bo > Bo* = 4.63462, the high spot is located in the interior of \mathcal{F} and asymptotes to the known location r=0.650312 for Bo $\to \infty$ and that for Bo < Bo* the high spot is on the boundary of \mathcal{F} .

To justify the numerical observation that for sufficiently small Bo the high spot is on the boundary, we remark that r=1 is always a critical point of $\xi_m(r)$ in [0,1] as a consequence of the Neumann boundary conditions. Furthermore, for $m \neq 0$, if r=1 is a local minimum, then we must have by continuity of $\xi_m(r)$ that there exists at least one local maximum in (0,1) since $\xi_m(0)=0$ and ξ_m is scaled such that $\xi_m(1)=1$. Thus we start by finding the concavity of ξ_m at r=1 and by determining Bo = Bo* for which $\xi_m''(1)=0$, i.e., where $\xi_m''(1)$ changes sign. To do so, we evaluate (4.2) for $m \geq 1$ at r=1 to get $\xi_m''(1)=m^2+\mathrm{Bo}(1-\omega^2\widehat{S}_r\xi_m(1))$. Here, we have used the fact that $\xi_m'(1)=0$ and that $\xi_m(1)=1$. Plugging in $\xi_m''(1)=0$ and noting that (ω,ξ_m) depends on Bo, we define

$$T(\mathrm{Bo}) = \frac{m^2}{\omega^2 \widehat{S}_r \xi_m(1) - 1}$$

and seek fixed points $\mathrm{Bo}^* = T(\mathrm{Bo}^*)$. The map $T(\mathrm{Bo})$ with m=1 is plotted in Figure 7(a) in blue, and the fixed point is the intersection with the black dashed line $y=\mathrm{Bo}$. Intuitively, to find the fixed points of $T(\mathrm{Bo})$ one would consider the iterative scheme $\mathrm{Bo}_{n+1} = T(\mathrm{Bo}_n)$. However, it is obvious from the slope at the fixed point in Figure 7(a) that these iterations will diverge. Additionally, we observe that $T(\mathrm{Bo})$ has a discontinuity where the denominator is zero. It follows naturally to instead consider the reciprocal map 1/T(1/x), where $x=1/\mathrm{Bo}$, shown in Figure 7(b) for m=1. This eliminates the observed discontuinity, but $x_{n+1}=1/T(1/x_n)$ would still diverge away from the fixed point. Therefore, instead of iterating along a horizontal line from the map $1/T(1/x_n)$ to the line $x_{n+1}=x_n$ we iterate along a line passing through $(x_n, 1/T(1/x_n))$ with slope α to the line $x_{n+1}=x_n$, as illustrated by the red arrows in Figure 7(b). We note that $\alpha=0$ simply corresponds to a horizontal line which returns the classical cobweb scheme. Additionally, we see that if $\alpha=1$, then the line we are iterating along is parallel to the line $x_{n+1}=x_n$ and the scheme is not sensible.

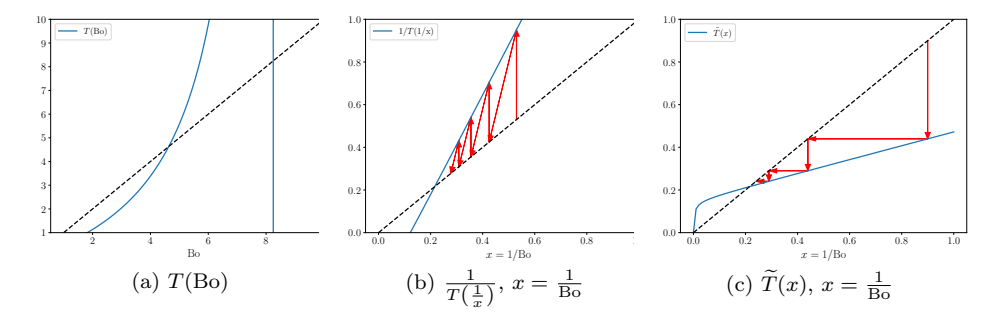


FIG. 7. (a) T(Bo) plotted for $Bo \in [1,10]$ and m=1, where the fixed point is the intersection with the black dashed line y=Bo. We note the discontinuity of T(Bo). (b) Reciprocal map 1/T(1/x) with x=1/Bo together with the modified fixed point iteration with slope $\alpha=3$. (c) New map $\widetilde{T}(x)$ with x=1/Bo (blue) plotted for $x \in (0,1]$ or $Bo \in [1,\infty)$, m=1, and $\alpha=3$, where we note a fixed point for finite Bo at the intersection with the black dashed line y=x together with the fixed point iteration.

With this idea, we define a new continuous map $\widetilde{T}:(0,\infty)\to(0,\infty)$ given by

(5.1)
$$\widetilde{T}(x) = \frac{1}{1 - \alpha} \left(\frac{1}{T\left(\frac{1}{x}\right)} - \alpha x \right),$$

shown in Figure 7(c) with m=1, $\alpha=3$, and now consider the iterative scheme $x_{n+1}=\widetilde{T}(x_n)$, as illustrated by the red arrows in Figure 7(c). The following lemma follows by simple computations.

LEMMA 5.1. For $\alpha > 1$, Bo* is a fixed point of T if and only if $x^* = \frac{1}{\text{Bo}^*}$ is a fixed point of \widetilde{T} .

Algorithm 5.1 outlines the procedure to determine the value for Bo*, the fixed point of T(Bo), using the map $\tilde{T}(x)$ and the equivalence of Lemma 5.1. To evaluate $\hat{S}_r \xi_m(1)$, we use the polynomial approximation derived in subsection 4.1 to write

(5.2)
$$\widehat{S}_r \xi_m(1) = \sum_{j=1}^n a_j^m \left(\widehat{S}_r h_j^m(1) + \beta_j^m \widehat{S}_r h_{j+1}^m(1) \right),$$

where $\widehat{S}_r h_j^m(1) = \frac{\mu_j^m}{2\pi \left(j + m - \frac{1}{2}\right)\left(j - \frac{1}{2}\right)}$; see Appendix B for details.

Algorithm 5.1 Procedure to determine Bo*

```
Input: Bo > 1, \alpha > 1, m \in \mathbb{N}
x_0 \leftarrow 1/\text{Bo}
while |x_{n+1} - x_n| >threshold do
Solve (3.5) for (\omega^2, \xi_m) with Bo = 1/x_n
Evaluate \omega^2 \widehat{S}_r \xi_m(1) using (5.2)
x_n \leftarrow \widetilde{T}(x_n)
end while
return 1/x_n
```

In Table 3, we report on the number of steps for Algorithm 5.1 to converge with a threshold of 10^{-14} for $\alpha = \{2, 3, 5, 10\}$ and m = 1, 2, 3, 4, 5. As the number of steps was similar for all the n tested, we only give the results for n = 20. We note that the classical fixed point iteration corresponds to $\alpha = 0$ and the modified fixed point iteration should converge for any $\alpha > 1$, although it is expected that more iterations are necessary for convergence for larger α .

Values of Bo* against the dimension of the solution space, $n \in \{5, 20, 80\}$, and the azimuthal mode, m = 1, 2, 3, 4, 5, are given in Table 4. We note the agreement between the column m = 1 and the value given in Figure 2(b).

Table 3

Number of steps for Algorithm 5.1 to converge (with threshold = 10^{-14}) to a fixed point for $\alpha = \{2, 3, 5, 10\}$, m = 1, 2, 3, 4, 5, and n = 20. All other values of n tested produced similar results.

	m = 1	m=2	m=3	m=4	m=5
$\alpha = 2$	29	40	92	195	540
$\alpha = 3$	30	94	194	395	1066
$\alpha = 5$	76	198	392	783	2088
$\alpha = 10$	184	450	873	1726	4568

Table 4 Values of Bo* for $n \in \{5, 20, 80\}$ and azimuthal mode m = 1, 2, 3, 4, 5.

	m = 1	m=2	m = 3	m=4	m=5
n=5	4.6342188	7.1574495	7.8108948	6.6284730	3.6110536
n = 20	4.6346165	7.1588900	7.8137285	6.6328709	3.6171135
n = 80	4.6346167	7.1588910	7.8137311	6.6328760	3.6171218

Before we prove our main result about high spots for the circular hole IFP, we collect two properties of the map \widetilde{T} based on our numerical results in the following lemma; see Figure 7(c).

Numerical Observation 5.2. For m=1,2,3,4,5, the map \widetilde{T} has a unique fixed point $x^*<1$. Moreover, $\widetilde{T}(x)>x$ whenever $x< x^*$, and $\widetilde{T}(x)< x$ whenever $x>x^*$.

THEOREM 5.3. Assume the map \widetilde{T} satisfies the two properties from Numerical Observation 5.2. For m = 1, 2, 3, 4, 5, define ξ_m to be the corresponding fundamental sloshing profile:

- (i) For Bo \in (Bo*, ∞), the high spot of ξ_m is located in the interior of \mathcal{F} .
- (ii) For Bo \in [1, Bo*), ξ_m has a local maximum at r = 1.

Proof. We note that, since $\xi_m(0) = 0$ and $\xi_m(r) \geq 0$, r = 0 is always a global minimum.

- (i) Recall that $x = \frac{1}{\text{Bo}}$. Using Numerical Observation 5.2 and the definition of \widetilde{T} , we have $\frac{1/T(\text{Bo}) \alpha/\text{Bo}}{1-\alpha} > \frac{1}{\text{Bo}}$, and since $\alpha > 1$, this simplifies to $\frac{1}{T(\text{Bo})} < \frac{1}{\text{Bo}}$. Therefore, $\frac{\omega^2 \widehat{S}_r \xi_m(1) 1}{m^2} < \frac{1}{\text{Bo}}$ so that $\xi_m''(1) = m^2 + \text{Bo}(1 \omega^2 \widehat{S}_r \xi_m(1)) > 0$. Thus $\xi_m''(1) > 0$, and along with the Neumann boundary conditions this implies that ξ_m has a local minimum at r = 1 and the high spot is in the interior of \mathcal{F} .
- (ii) Using similar calculations as above, we establish that $\xi''_m(1) < 0$. Since $\xi'_m(1) = 0$, we have that a local maximum occurs at r = 1.

Remark 5.4. For m=1,2,3,4,5 and for Bo $\in [1, \mathrm{Bo}^*)$, we observe numerically that there are no other critical points of ξ_m in (0,1). This implies that r=1 is a global maximum of ξ_m , and thus the high spot of ξ_m is on the boundary of \mathcal{F} .

Remark 5.5. When Bo $\to \infty$, Theorem 5.3 implies that the high spot is in the interior of \mathcal{F} for the circular hole IFP without surface tension. This is consistent with previous results on the infinite parallel strip IFP [16, Proposition 2.7] as well as the circular hole IFP [16, Theorem 3.2] where the authors neglected surface tension.

For further illustration, Figure 8 shows the location of the first two nonzero roots of $\xi_1(r)$ for all Bo \in [0.1, 1000], one of them always being r=1. The derivative is expressed analytically as $\xi'_1(r) = \sum_{j=1}^n a_j^1 \frac{d}{dr} q_j^1(r)$, where the radial polynomial derivative uses derivatives of Jacobi polynomials and a simple root solver is used to find the zeros. Figure 8 shows the expected horizontal asymptote y=0.650312, the expected horizontal line r=1, and the expected critical Bo*, where both curves intersect. For Bo < Bo*, since the blue curve is always above the orange line (see Figure 8(b) for a blow-up plot), we conclude that there are no critical points in (0,1).

6. Discussion. This paper provides the first study on the IFP including surface tension effects. Although the geometries considered are the infinite parallel strip and the circular hole, for any Bo, the results give an upper bound for the fundamental

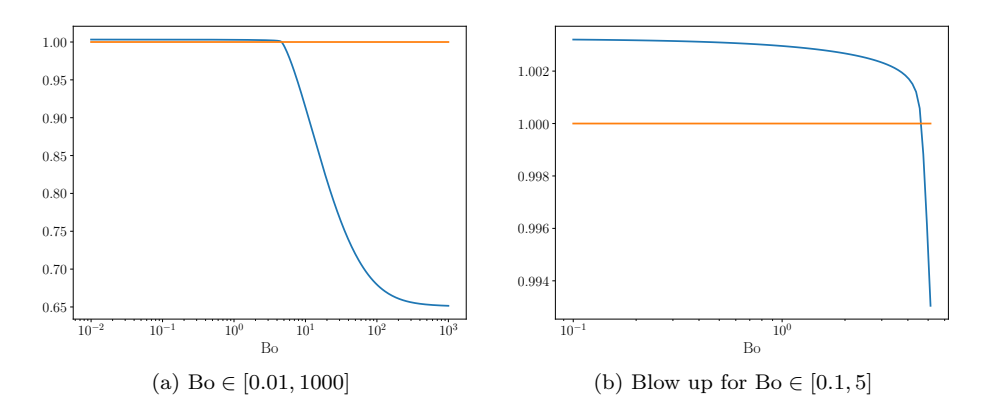


Fig. 8. Location of the first two zeros of $\xi'_1(r)$ as a function of Bo. Because of the Neumann boundary conditions, r=1 is always a zero and corresponds to the orange line. The blue curve is obtained by numerically finding the first zero of $\xi'_1(r)$.

sloshing frequency for any container with the same free surface [26]. Building on previous studies without surface tension [5, 10], we derive an integro-differential equation (2.4) and prove the spectrum is equivalent to the spectrum of (2.1). The benefit of this approach is that, for the considered geometries, the problem is transformed from an unbounded domain to a bounded one-dimensional domain. We numerically solve it by expanding in a polynomial basis, suitably chosen to satisfy the boundary conditions. We derive a closed form expression for the eigenvalue problem, which is a generalized eigenvalue matrix equation, and numerically approximate it.

We have assumed the free-end edge constraint; i.e., the contact line slips freely along the vertical wall (edge of the ice hole) while intersecting it orthogonally. However, experimental evidence [4, 6] reveals that the dynamic behavior of the contact line depends crucially on the contact angle, i.e., the angle where the free surface meets a solid surface. It would be interesting to consider either the pinned-end edge constraint [2] or other dynamic contact line boundary conditions such as Hocking's linear wetting boundary condition [11, 12], Dussan's nonlinear contact line model incorporating static contact angle hysteresis [6], or a combination of Hocking's and Dussan's model that was recently proposed by Viola, Brun, and Gallaire [30, 31].

The eigenvalues from the IFP are upper bounds for the corresponding eigenvalues for all other containers with coinciding free surface. It would therefore be of interest to know if the approximate eigenvalues presented here are perhaps upper or lower bounds for the true eigenvalues of IFP. In the absence of surface tension this was indeed considered in [8, 10]. The methods for the upper bounds were summarized in section 1. For the lower bounds, Henrici, Troesch, and Wuytack [10] utilized the domain monotonicity property along with an infinitely deep cylinder or trough to bound the eigenvalues from below. When appropriate, they improved the bound by implementing the Krylov-Bogoliubov inequality on the integral operator to provide a tighter lower bound. Fox and Kuttler [8] used the method of intermediate problems on an equivalent weighted problem on a region where solutions are known. Taking advantage of known eigenvectors of the unweighted sloshing problem on the simple region, Fox and Kuttler [8] produced much tighter lower bounds than otherwise observed while using low-dimensional matrices. While the domain monotonicity property holds when including surface tension, the other properties mentioned do not necessarily extend to the model considered here. Nonetheless, numerically bounding

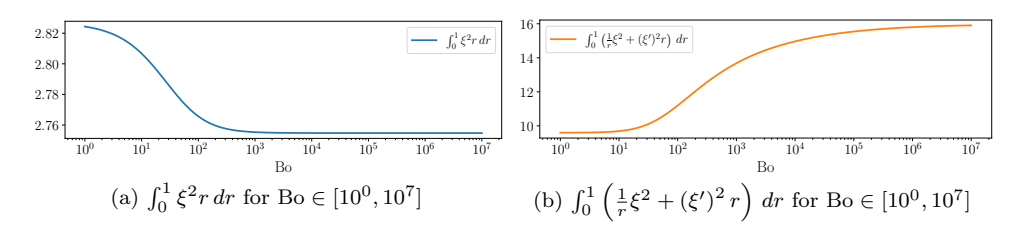


Fig. 9. Comparison of the different contributions to the free surface energy to illustrate how the fundamental sloshing profile minimizes one versus the other depending on Bo with m = 1.

eigenvalues would be a significant advantage to this study and could be investigated in future work.

We numerically study how the location of the high spot for the IFP depends on Bo. Using a simple fixed point iteration we determine the value of Bo such that for any lower Bo the high spot is on the boundary of the free surface \mathcal{F} . This result compliments previous work [16] which shows that the high spot is always in the interior of \mathcal{F} for the IFP in the absence of surface tension. For physical intuition, we recall that the fundamental sloshing profile for the circular hole IFP minimizes the free surface energy,

$$\frac{\int_0^1 \xi_m^2 r \, dr + \frac{1}{\text{Bo}} \int_0^1 \left(\frac{m^2}{r} \xi_m^2 + \left(\xi_m' \right)^2 r \right) dr}{\int_0^1 \widehat{S}_r \xi_m(r) \xi_m(r) r \, dr}.$$

For simplicity, we scale the solution such that $\int_0^1 \widehat{S}_r \xi_m(r) \xi_m(r) r \, dr = 1$. For large Bo we are primarily minimizing $\int_0^1 \xi_m^2 r \, dr$, whereas for small Bo we are primarily minimizing $\int_0^1 (\frac{m^2}{r} \xi_m^2 + (\xi_m')^2 r) \, dr$. These different contributions to the free surface energy are shown in Figure 9 for m = 1. Therefore, we pay a more significant penalty for variation in the derivative when Bo is small and the intuition is that sloshing profiles with no interior extrema suffer less from this penalty. Motivated by this observation, we conjecture that, for any shape domain, given sufficiently small Bo, the high spot is located on the boundary of the free surface.

Appendix A. Matrix elements computations. The coefficients M_{ij}^m follow immediately from the orthogonality of the h_j^m polynomials, and computation for \tilde{L}_{ij}^m can be found in [20]. Therefore, here we focus on showing that the stiffness matrix is diagonal and on finding the values for those coefficients.

We first define $\tilde{K}^m_{ij} = \int_0^1 (\frac{m^2}{r} h_j^m h_i^m + (h_j^m)'(h_i^m)'r) dr$ so that we have $K^m_{ij} = \tilde{K}^m_{ij} + \beta^m_i \tilde{K}^m_{i+1,j} + \beta^m_j \tilde{K}^m_{i,j+1} + \beta^m_i \beta^m_j \tilde{K}^m_{i+1,j+1}$. Now we compute the \tilde{K}^m_{ij} elements and start by recalling that $h^m_j = \mu^m_j r^m p^{(0,m)}_{j-1} (2r^2 - 1)$. From [22, Eq. 18.9.15] we have that $(h^m_j)' = \frac{m}{r} h^m_j + 2\mu^m_j r^{m+1} (m+j) p^{(1,m+1)}_{j-2} (2r^2 - 1)$, and substituting this along with the definition of h^m_j into \tilde{K}_{ij} , we obtain

$$\tilde{K}_{ij}^{m} = 2\mu_{j}^{m}\mu_{i}^{m}\left(m^{2}A_{ij}^{m} + \frac{m}{\mu_{j}^{m}}(i+m)B_{ij}^{m} + \frac{m}{\mu_{i}^{m}}(j+m)B_{ji}^{m} + (j+m)(i+m)C_{ij}^{m}\right),$$

where

$$\begin{split} A^m_{ij} &= \int_0^1 r^{m-1} p_{j-1}^{(0,m)} (2r^2 - 1) r^{m-1} p_{i-1}^{(0,m)} (2r^2 - 1) r \, dr, \\ B^m_{ij} &= \int_0^1 h_j^m r^m p_{i-2}^{(1,m+1)} (2r^2 - 1) \, dr, \\ C^m_{ij} &= 2 \int_0^1 r^{m+1} p_{j-2}^{(1,m+1)} (2r^2 - 1) r^{m+1} p_{i-2}^{(1,m+1)} (2r^2 - 1) \, dr. \end{split}$$

To simplify A_{ij}^m we relate the $p_{j-1}^{(0,m)}$ Jacobi polynomials to the $p_{j-1}^{(0,m-1)}$ Jacobi polynomials in order to use the orthogonality of the h_j^{m-1} polynomials. First use the symmetry relation [22, Table 18.6.1] and then the connection sum formula [22, Eq. 18.18.14], with $\gamma = m$, $\alpha = m - 1$, and $\beta = 0$, to get

$$p_{j-1}^{(0,m)}(x) = (-1)^j \frac{(j-1)!}{(m+1)_{j-1}} \sum_{\ell=1}^j \frac{m+2(\ell-1)}{m} \frac{(m)_{\ell-1}}{(\ell-1)!} (-1)^\ell p_{\ell-1}^{(0,m-1)}(x).$$

Since $m + 2(\ell - 1) = \frac{1}{2}(\mu_{\ell}^{m-1})^2$, we have

(A.1)
$$r^{m-1}p_{j-1}^{(0,m)}(2r^2-1) = \frac{(-1)^j}{m} \frac{(j-1)!}{(m+1)_{j-1}} \sum_{\ell=1}^j \frac{\mu_\ell^{m-1}}{2} \frac{(m)_{\ell-1}}{(\ell-1)!} (-1)^\ell h_\ell^{m-1}.$$

Let $\kappa_{ij}^m = (-1)^{i+j} \frac{(j-1)!(i-1)!}{(m+1)_{j-1}(m+1)_{i-1}}$ and $\nu = \min(i,j)$; then we have

$$A^m_{ij} = \frac{\kappa^m_{ij}}{m^2} \sum_{\ell=1}^j \sum_{k=1}^i \frac{\mu^{m-1}_\ell \mu^{m-1}_k}{4\kappa^{m-1}_{\ell k}} \delta_{\ell k} = \frac{\kappa^m_{ij}}{m^2} \sum_{\ell=0}^{\nu-1} (m+2\ell) \left(\frac{(m)_\ell}{\ell!}\right)^2 = \frac{\kappa^m_{ij}}{m} \left(\frac{(m+1)_{\nu-1}}{(\nu-1)!}\right)^2.$$

The last simplification follows from $(\frac{(\nu-1)!}{(m+1)_{\nu-1}})^2 \sum_{\ell=0}^{\nu-1} (m+2\ell) (\frac{(m)_\ell}{\ell!})^2 = m$, which can be easily proved by induction on ν . Therefore,

$$A_{ij}^{m} = \frac{(-1)^{i+j}}{2m} \frac{(\min(i,j))_{m}}{(\max(i,j))_{m}}.$$

Next, we turn to B_{ij}^m and start by again using the connection sum formula [22, Eq. 18.18.14], this time with $\gamma = 1$, $\alpha = 0$, and $\beta = m$, to note that

(A.2)
$$r^m p_{i-1}^{(1,m)}(2r^2 - 1) = \frac{1}{2(m+i)} \sum_{\ell=1}^i \mu_\ell^m h_\ell^m(x).$$

Therefore, using the contiguous relation [22, Eq. 18.9.3] for $p_{i-2}^{(1,m+1)}$ along with the above relation for $r^m p_{i-1}^{(1,m)}$ and (A.1) for $r^m p_{j-1}^{(0,m+1)}$, we have

$$r^{m} p_{i-2}^{(1,m+1)}(2r^{2}-1) = \frac{1}{2} \sum_{\ell=1}^{i} \frac{1}{m+i} \left(1 - (-1)^{i+\ell} \frac{(\ell)_{m}}{(i)_{m}} \right) \mu_{\ell}^{m} h_{\ell}^{m}(r).$$

From the orthogonality of h_i^m we now have

$$B_{ij}^{m} = \begin{cases} \frac{\mu_{j}^{m}}{2(m+i)} \left(1 - (-1)^{i+j} \frac{(j)_{m}}{(i)_{m}}\right) & \text{if } j < i, \\ 0 & \text{if } j \ge i. \end{cases}$$

Lastly, we turn to C_{ij}^m and use (A.2) for $r^{m+1}p_{j-2}^{(1,m+1)}$ so that we can again use the orthogonality of the h_j^m polynomials. After simplifying we get

$$C_{ij}^m = \frac{\min(i,j) - 1}{\max(i,j) + m}.$$

With these expressions for A_{ij}^m , B_{ij}^m , and C_{ij}^m we now have that

$$\tilde{K}_{ij}^{m} = \mu_{i}^{m} \mu_{i}^{m} \left(m + 2(\min(i, j) - 1)(\min(i, j) + m) \right)$$

Let us write the stiffness matrix as $K^m_{ij} = \Omega^m_{ij} + \beta^m_i \Omega^m_{i+1,j}$ with $\Omega^m_{ij} = \tilde{K}^m_{ij} + \beta^m_j \tilde{K}^m_{i,j+1}$. Due to the symmetry of \mathbf{K} we assume without loss of generality that j < i such that $\tilde{K}^m_{ij} = \mu^m_j \mu^m_i \ (m+2(j-1)(j+m))$. Then, from the definition of β^m_j we have that $\Omega^m_{ij} = 0$ and $\Omega^m_{i,j+1} = 0$ if $j \neq i$. In the case that i = j it follows from direct calculation that $K^m_{jj} = -\mu^m_j \mu^m_{j+1} (\mu^{m+1}_j)^2 \beta^m_j$.

Appendix B. Integral operator evaluated at r = 1. We start with the Hankel transform of h_i^m , given in [20], to determine that

$$\widehat{S}_r h_j^m(1) = (-1)^{j-1} \mu_j^m \int_0^\infty \frac{J_{2j+m-1}(k)J_m(k)}{k} dk.$$

Using the Weber–Schafheitlin formula [22, Eq. 10.22.57], with $a=1=\lambda, \, \mu=2j+m-1$, and $\nu=m$, we have

$$\int_{0}^{\infty} \frac{J_{2j+m-1}(k)J_{m}(k)}{k} dk = \frac{\Gamma\left(j+m-\frac{1}{2}\right)}{2\Gamma\left(\frac{3}{2}-j\right)\Gamma\left(j+\frac{1}{2}\right)\Gamma\left(j+m+\frac{1}{2}\right)},$$
$$= \frac{(-1)^{j}}{2\pi\left(j+m-\frac{1}{2}\right)\left(\frac{1}{2}-j\right)},$$

where we have simplified in a similar fashion as done in [20]. It follows that

$$\widehat{S}_r h_j^m(1) = \frac{\mu_j^m}{2\pi \left(j + m - \frac{1}{2}\right) \left(j - \frac{1}{2}\right)}.$$

Acknowledgments. We would like to thank Akil Narayan and Fernando Guevara Vasquez for helpful conversations. We would also like to thank the anonymous referees for carefully reading the manuscript and for useful suggestions.

REFERENCES

- F. AUTERI, N. PAROLINI, AND L. QUARTAPELLE, Essential imposition of Neumann condition in Galerkin-Legendre elliptic solvers, J. Comput. Phys., 185 (2003), pp. 427–444, https://doi.org/10.1016/S0021-9991(02)00064-5.
- T. B. BENJAMIN AND J. C. SCOTT, Gravity-capillary waves with edge constraints, J. Fluid Mech., 92 (1979), pp. 241–267, https://doi.org/10.1017/S0022112079000616.
- [3] C. CANUTO, M. Y. HUSSAINI, A. QUARTERONI, AND T. A. ZANG JR, Spectral Methods in Fluid Dynamics, Springer, Berlin, 1988, https://doi.org/10.1007/978-3-642-84108-8.
- [4] B. COCCIARO, S. FAETTI, AND C. FESTA, Experimental investigation of capillarity effects on surface gravity waves: Non-wetting boundary conditions, J. Fluid Mech., 246 (1993), pp. 43–66, https://doi.org/10.1017/S0022112093000035.
- [5] A. DAVIS, Waves in the presence of an infinite dock with gap, IMA J. Appl. Math, 6 (1970), pp. 141–156, https://doi.org/10.1093/imamat/6.2.141.

- [6] E. DUSSAN, On the spreading of liquids on solid surfaces: Static and dynamic contact lines, Annu. Rev. Fluid Mech., 11 (1979), pp. 371–400, https://doi.org/10.1146/annurev.fl.11. 010179.002103.
- [7] O. M. FALTINSEN AND A. N. TIMOKHA, Sloshing, Cambridge University Press, Cambridge, UK, 2009.
- [8] D. W. FOX AND J. R. KUTTLER, Sloshing frequencies, Z. Angew. Math. Phys., 34 (1983), pp. 668-696, https://doi.org/10.1007/BF00948809.
- [9] B.-Y. Guo and L.-L. Wang, Jacobi approximations in non-uniformly Jacobi-weighted Sobolev spaces, J. Approx. Theory, 128 (2004), pp. 1–41, https://doi.org/10.1016/j.jat.2004.03.008.
- [10] P. HENRICI, B. A. TROESCH, AND L. WUYTACK, Sloshing frequencies for a half-space with circular or strip-like aperture, Z. Angew. Math. Phys., 21 (1970), pp. 285–318, https://doi.org/10.1007/BF01627938.
- [11] L. HOCKING, The damping of capillary-gravity waves at a rigid boundary, J. Fluid Mech., 179 (1987), pp. 253–266, https://doi.org/10.1017/S0022112087001514.
- [12] L. HOCKING, Waves produced by a vertically oscillating plate, J. Fluid Mech., 179 (1987), pp. 267–281, https://doi.org/10.1017/S0022112087001526.
- [13] R. A. IBRAHIM, Liquid Sloshing Dynamics: Theory and Applications, Cambridge University Press, Cambridge, UK, 2005, https://doi.org/10.1017/CBO9780511536656.
- [14] N. D. KOPACHEVSKY AND S. G. KREIN, Operator Approach to Linear Problems of Hydrodynamics: Volume 1: Self-adjoint Problems for Ideal Fluids, Oper. Theory Adv. Appl. 128, Birkhäuser, Basel, 2001, https://doi.org/10.1007/978-3-0348-8342-9.
- [15] V. KOZLOV AND N. KUZNETSOV, The ice-fishing problem: The fundamental sloshing frequency versus geometry of holes, Math. Methods Appl. Sci., 27 (2004), pp. 289–312, https://doi. org/10.1002/mma.442.
- [16] T. KULCZYCKI AND N. KUZNETSOV, 'High spots' theorems for sloshing problems, Bull. Lond. Math. Soc., 41 (2009), pp. 494–505, https://doi.org/10.1112/blms/bdp021.
- [17] T. KULCZYCKI AND N. KUZNETSOV, On the 'high spots' of fundamental sloshing modes in a trough, Proc. R. Soc. A., 467 (2011), pp. 1491–1502, https://doi.org/10.1098/rspa.2010. 0258.
- [18] T. KULCZYCKI AND M. KWAŚNICKI, On high spots of the fundamental sloshing eigenfunctions in axially symmetric domains, Proc. Lond. Math. Soc., 105 (2012), pp. 921–952, https: //doi.org/10.1112/plms/pds015.
- [19] L. LANDAU, Bessel functions: Monotonicity and bounds, J. Lond. Math. Soc. (2), 61 (2000), pp. 197–215.
- [20] J. W. MILES, On the eigenvalue problem for fluid sloshing in a half-space, Z. Angew. Math. Phys., 23 (1972), pp. 861–869, https://doi.org/10.1007/BF01596214.
- [21] N. N. Moiseev, Introduction to the theory of oscillations of liquid-containing bodies, Adv. Appl. Mech., 8 (1964), pp. 233–289, https://doi.org/10.1016/S0065-2156(08)70356-9.
- [22] F. W. J. Olver, A. B. Olde Daalhuis, D. W. Lozier, B. I. Schneider, R. F. Boisvert, C. W. Clark, B. R. Miller, B. V. Saunders, H. S. Cohl, and M. A. McClain, EDS, NIST Digital Library of Mathematical Functions, Release 1.1.5 of 2022-03-15, 2022, http://dlmf.nist.gov.
- [23] R. PIESSENS, Hankel transform, in The Transforms and Applications Handbook, 3rd ed., CRC Press, Boca Raton, FL, 2000, pp. 9-1-9-16, https://doi.org/10.1201/9781315218915.
- [24] Polymath?: Establishing the hot spots conjecture for acute-angled triangles, https://asone.ai/polymath/index.php?title=The_hot_spots_conjecture.
- [25] J. SHEN, Efficient spectral-Galerkin method i. direct solvers of second-and fourth-order equations using Legendre polynomials, SIAM J. Sci. Comput., 15 (1994), pp. 1489–1505, https://doi.org/10.1137/0916006.
- [26] C. H. TAN, C. HOHENEGGER, AND B. OSTING, A variational characterization of fluid sloshing with surface tension, SIAM J. Appl. Math., 77 (2017), pp. 995–1019, https://doi.org/10. 1137/16M1104330.
- [27] C. H. TAN, C. HOHENEGGER, AND B. OSTING, An Isoperimetric Sloshing Problem in a Shallow Container With Surface Tension, preprint, arXiv:2011.03766, 2021, https://arxiv.org/abs/ 2111.03766.
- [28] B. TROESCH, Sloshing frequencies in a half-space by Kelvin inversion, Pac. J. Math., 47 (1973), pp. 539–552, https://doi.org/10.2140/pjm.1973.47.539.
- [29] J. VANNEKOSKI, The Method of Layer Potentials: Unique Solvability of the Dirichlet Problem for Laplace's Equation in C¹-Domains With L^p-Boundary Data, Ph.D. thesis, University of Helsinki, Helsinki, Finland, 2014.
- [30] F. VIOLA, P.-T. BRUN, AND F. GALLAIRE, Capillary hysteresis in sloshing dynamics: A weakly nonlinear analysis, J. Fluid Mech., 837 (2018), pp. 788–818, https://doi.org/10.1017/jfm. 2017.860.

- [31] F. VIOLA AND F. GALLAIRE, Theoretical framework to analyze the combined effect of surface tension and viscosity on the damping rate of sloshing waves, Phys. Rev. Fluids, 3 (2018), 094801, https://doi.org/10.1103/PhysRevFluids.3.094801.
- [32] K. Wang, On the Neumann problem for harmonic functions in the upper half plane, J. Math. Anal. Appl., 419 (2014), pp. 839–848, https://doi.org/10.1016/j.jmaa.2014.04.076.